NUMERICAL SIMULATIONS OF HEAT TRANSFER IN AN ANNULAR FUEL CHANNEL WITH THREE-DIMENSIONAL SPACER RIBS SET UP PERIODICALLY UNDER A FULLY DEVELOPED TURBULENT FLOW

June 1996

Kazuyuki TAKASE and Norio AKINO

日 本 原 子 力 研 究 所
Japan Atomic Energy Research Institute

Numerical Simulations of Heat Transfer in an Annular Fuel Channel
with Three-dimensional Spacer Ribs Set Up Periodically under
a Fully Developed Turbulent Flow

Kazuyuki TAKASE and Norio AKINO

Department of Advanced Nuclear Heat Technology
Oarai Research Establishment
Japan Atomic Energy Research Institute
Tokai-mura, Naka-gun, Ibaraki-ken

Thermal-hydraulic characteristics of an annular fuel channel with spacer ribs for high temperature gas-cooled reactors were analyzed numerically by three-dimensional heat transfer computations under a fully developed turbulent flow. The two-equations κ-ε turbulence model was applied to the present turbulent analysis. In particular, the κ-ε turbulence model constants and the turbulent Prandtl number were improved from the previous standard values proposed by Jones and Launder in order to obtain heat transfer predictions with higher accuracy. Consequently, heat transfer coefficients and friction factors in the spacer-ribbed fuel channel were predicted with sufficient accuracy in the range of Reynolds number exceeding 3000. It was clarified quantitatively from the present study that main mechanism for the heat transfer augmentation in the spacer-ribbed fuel channel was combined effects of the turbulence promoter effect by the spacer ribs and the velocity acceleration effect by a reduction in the channel cross-section.

周期的に設置された3次元スペーサリブを有する環状燃料チャンネル内
の十分に発達した乱流場における熱伝達の数値解析

日本原子力研究所大洗研究所核熱利用研究部
高瀬 和之・秋野 詔夫

　高温ガス炉で使用されるスペーサリブ付き環状燃料チャンネルの伝熱流動特性を，十分に発達した乱流場のもとで3次元熱流動計算を行って数値的に解析した。乱流計算にはκ-ε2方程式乱流モデルを使用した。今回は，より高精度の熱伝達予測値を得るために，κ-ε乱流モデル定数と乱流プラントル数をJonesとLaunderが提案した標準値から改良した。その結果，スペーサリブ付き燃料チャンネルの熱伝達率と摩擦係数は3000以上のレイノルズ数に対して十分な精度で予測できた。本研究により，スペーサリブ付き燃料チャンネルの伝熱促進機構は，スペーサリブによるタービュレンスプロモータ効果と流路断面積縮小による加速流効果の複合したものであることが定量的に明らかになった。

東海研究所：〒319－11 茨城県那珂郡東海村白方白根2－4

Contents

目　　　　次

1. INTRODUCTION

Japan Atomic Energy Research Institute has been constructing a High Temperature Engineering Test Reactor (HTTR) to establish and upgrade the technological basis for advanced Very High-temperature Gas-cooled Reactors (VHTRs) and to conduct various irradiation tests for innovative high temperature basic researches. HTTR is a helium-cooled, graphite-moderated reactor with a core inlet temperature of 395°C, maximum core outlet temperature of 950°C, pressure of 4 MPa, thermal power of 30 MW and power density of 2.5 MW/m³. The pressure vessel of HTTR shown in Fig. 1 has a height of 13.2 m and a diameter of 5.5 m, and contains the active core, permanent and replaceable reflectors, core support structure and core restraint mechanism. The active core consists of 30 fuel columns and 7 control-rod guide columns, each of which is composed of 5 hexagonal graphite blocks stacked vertically. The dimensions of the graphite block is 360 mm in width across flats and 580 mm in height. Figure 2 shows the fuel element consisted of the graphite block and 33 fuel holes. A standard fuel rod with spacer ribs on its outer surface is inserted into each fuel hole. Helium gas flows downward through each annular fuel channel between the fuel hole with a diameter of 41 mm, Do, and the fuel rod with an external diameter of 34 mm, Di. Thus, the fuel channel has a hydraulic diameter, $De=Do-Di$, of 7 mm and an annulus ratio, Di/Do, of 0.829. In addition, the bulk Reynolds number, Re, at the inlet of the fuel channel is less than 10000 and that at the outlet of the fuel channel is more than 3000.

The turbulent heat transfer characteristics in the fuel channels for VHTRs have been studied experimentally by Kays and Leung[1], Dalle Donne and Meerwald[2] and Wilson and Medwell[3] in the case of a concentric smooth annulus. Furthermore, Dalle Donne and Meyer[4] examined the turbulent heat transfer coefficients of the fuel channel with transverse square ribs and Hassan and Rehme[5] investigated the heat transfer performance in rod bundles with spacer grids. However, all of the experimental conditions of the previous researches, such as temperature, pressure, Re, heat flux, Di/Do and channel geometry do not simulate the HTTR operational conditions. As shown in Fig. 2, the fuel rod for HTTR has 9 trapezoidal-spacer ribs on its outer surface so as to keep the annulus concentricity. From the viewpoint of the thermal design in HTTR, it is very difficult to predict the turbulent heat transfer characteristics of the spacer-ribbed fuel channels used in the HTTR core from the results of previous researches with different experimental conditions from those of HTTR.

Then, heat transfer coefficients and friction factors in the spacer-ribbed fuel channels were investigated experimentally by Takase[6] under the same helium gas conditions as the HTTR operation. On the basis of this experimental results, numerical analyses were carried out by 3-dimensional computations with the k-ε turbulence model in order to predict

quantitatively the turbulent heat transfer characteristics in annular fuel channels augmented by spacer ribs. In particular, constants of the k-ε turbulence model and the turbulent Prandtl number were improved from the previous standard values proposed by Jones and Launder[7] in order to obtain heat transfer predictions with higher accuracy. This paper describes the predicted results regarding the turbulent heat transfer characteristics in the spacer-ribbed fuel channels and also compares the predicted results with the experimental results.

2. NUMERICAL ANALYSIS

2.1 Governing Equations

The 3-dimensional continuity, Reynolds averaged Navier-Stokes and energy equations in an incompressible flow, and also the turbulence kinematic energy, k, and its dissipation rate, ε, computed from the two-equations k-ε model[7] can be written using Cartesian tensor notation as:

◆ Continuity equation

$$\frac{\partial}{\partial x_i}(\rho u_i) = 0 \tag{1}$$

◆ Raynolds averaged Navier-Stokes equation

$$\frac{\partial}{\partial x_j}(\rho u_i u_j) = -\frac{\partial p_p}{\partial x_i} + \frac{\partial}{\partial x_j}\left[\mu_{eff}\left(\frac{\partial u_i}{\partial x_j} + \frac{\partial u_j}{\partial x_i}\right)\right] + \beta - \frac{2}{3}\frac{\partial(\rho k)}{\partial x_i} \tag{2}$$

◆ Energy equation

$$\frac{\partial}{\partial x_i}(\rho u_i T_p) = \frac{\partial}{\partial x_i}\left(\frac{\mu_{eff}}{Pr_{eff}}\frac{\partial T_p}{\partial x_i}\right) \tag{3}$$

◆ k-equation

$$\frac{\partial}{\partial x_i}(\rho u_i k) = \frac{\partial}{\partial x_i}\left(\frac{\mu_t}{\sigma_k}\frac{\partial k}{\partial x_i}\right) + \mu_t\left(\frac{\partial u_i}{\partial x_j} + \frac{\partial u_j}{\partial x_i}\right)\frac{\partial u_i}{\partial x_i} - \rho\varepsilon \tag{4}$$

◆ ε-equation

$$\frac{\partial}{\partial x_i}(\rho u_i \varepsilon) = \frac{\partial}{\partial x_i}\left(\frac{\mu_t}{\sigma_\varepsilon}\frac{\partial \varepsilon}{\partial x_i}\right) + C_1\mu_t\frac{\varepsilon}{k}\left(\frac{\partial u_i}{\partial x_j} + \frac{\partial u_j}{\partial x_i}\right)\frac{\partial u_i}{\partial x_i} - C_2\rho\frac{\varepsilon^2}{k} \tag{5}$$

quantitatively the turbulent heat transfer characteristics in annular fuel channels augmented by spacer ribs. In particular, constants of the k-ε turbulence model and the turbulent Prandtl number were improved from the previous standard values proposed by Jones and Launder[7] in order to obtain heat transfer predictions with higher accuracy. This paper describes the predicted results regarding the turbulent heat transfer characteristics in the spacer-ribbed fuel channels and also compares the predicted results with the experimental results.

2. NUMERICAL ANALYSIS

2.1 Governing Equations

The 3-dimensional continuity, Reynolds averaged Navier-Stokes and energy equations in an incompressible flow, and also the turbulence kinematic energy, k, and its dissipation rate, ε, computed from the two-equations k-ε model[7] can be written using Cartesian tensor notation as:

♦ Continuity equation

$$\frac{\partial}{\partial x_i}(\rho u_i) = 0 \tag{1}$$

♦ Raynolds averaged Navier-Stokes equation

$$\frac{\partial}{\partial x_j}(\rho u_i u_j) = -\frac{\partial p_p}{\partial x_i} + \frac{\partial}{\partial x_j}\left[\mu_{e\!f\!f}\left(\frac{\partial u_i}{\partial x_j} + \frac{\partial u_j}{\partial x_i}\right)\right] + \beta - \frac{2}{3}\frac{\partial(\rho k)}{\partial x_i} \tag{2}$$

♦ Energy equation

$$\frac{\partial}{\partial x_i}(\rho u_i T_p) = \frac{\partial}{\partial x_i}\left(\frac{\mu_{e\!f\!f}}{Pr_{e\!f\!f}}\frac{\partial T_p}{\partial x_i}\right) \tag{3}$$

♦ k-equation

$$\frac{\partial}{\partial x_i}(\rho u_i k) = \frac{\partial}{\partial x_i}\left(\frac{\mu_t}{\sigma_k}\frac{\partial k}{\partial x_i}\right) + \mu_t\left(\frac{\partial u_i}{\partial x_j} + \frac{\partial u_j}{\partial x_i}\right)\frac{\partial u_i}{\partial x_i} - \rho\varepsilon \tag{4}$$

♦ ε-equation

$$\frac{\partial}{\partial x_i}(\rho u_i \varepsilon) = \frac{\partial}{\partial x_i}\left(\frac{\mu_t}{\sigma_\varepsilon}\frac{\partial \varepsilon}{\partial x_i}\right) + C_1\mu_t\frac{\varepsilon}{k}\left(\frac{\partial u_i}{\partial x_j} + \frac{\partial u_j}{\partial x_i}\right)\frac{\partial u_i}{\partial x_i} - C_2\rho\frac{\varepsilon^2}{k} \tag{5}$$

Here, each subscript of i, j, k corresponds to the coordinate (x, y, z) and 1, 2, 3, respectively. The effective viscosity, μ_{eff}, and the effective Prandtl number, Pr_{eff}, are given by $\mu_{eff} = \mu_t +$ μ; $\mu_t = C_\mu \rho k^2 / \varepsilon$; and $Pr_{eff} = \mu / Pr + \mu_t / Pr_t$.

Constants of the k-ε turbulence model used in the present study are $C_\mu = 0.09 \sim 0.12$; $C_1 = 1.44$; $C_2 = 1.92$; $\sigma_k = 1.0$; $\sigma_\varepsilon = 1.3$; and $Pr_t = 0.86 \sim 1.0$. Especially, C_μ and Pr_t were tuned up from 0.09 and 0.9 which were the previous standard values proposed by Jones and Launder[7] so as to obtain the predicted values with the sufficient accuracy in comparison with the experimental values.

On the other hand, the pressure, P, in the case of a periodic fully developed flow in the space direction is separated into two parts as proposed by Patankar, Liu, and Sparrow[8]: $P(x, y, z) = -\beta \ z + P_p(x, y, z)$; Here, $P_p(x, y, z)$ denotes the periodic parts of pressure; β is the pressure drop parameter during a one periodic length; and z is the axial distance from the spacer-ribbed fuel channel inlet.

2.2 Numerical and Boundary Conditions

Three-dimensional computations were performed in the spacer-ribbed fuel channel with a central angle of 120° as shown in Fig. 3. It simulated one-third of the spacer-ribbed fuel channel at an arbitrary axial distance between the annular fuel channel inlet and outlet. The numerical conditions were as follows: Fluid was helium gas with an initial temperature of 500°C and pressure of 4 MPa; Heat flux of the inner wall and spacer rib surface was varied from 38 to 252 kW/m^2 corresponding to the variation of Re from 3000 to 20000; Outer wall was insulated; Radiation from the inner to outer walls was considered; Emissivity of the inner wall and spacer rib surface was set to 0.8[9] and emissivity of the outer wall was set to 0.3[10]; Wall conduction was neglected; and constant thermophysical properties were assumed for the working fluid.

Figure 3 shows the analytical model and boundary conditions. The u, v and w are the fluid velocity components corresponding to x, y and z directions, respectively, and those are zero at the walls. To obtain a fully developed turbulent flow at the inlet of the computational domain, periodic boundary conditions are set at the inlet and outlet sections. Calculated values of the velocities and turbulence quantities at the outlet section were substituted as the inlet conditions for the next iteration. Symmetric boundary conditions were set to both circumferential ends of the computational domain. Here, the sector angle, θ, between the symmetric boundary and the center of the spacer rib was 60°.

The wall function proposed by Launder and Spalding[11] was used to prescribe the boundary conditions along the channel walls. The near-wall dissipation value was set as $\varepsilon = C_\mu^{3/4} k^{3/2} / \kappa y_p$ from the equilibrium assumption in which the production and dissipation of

the turbulence were equal. Here, κ is the Karmann's constant and y_p is the normal distance from the wall to the adjacent grid point. The wall gradient of k was also set to be zero. The wall temperature, T_w, was obtained from the following formulation of Launder and Spalding[11] that was based on the analogy between heat and momentum transfers.

$$T_w = q_w T^+ / \rho c_p C_\mu^{1/4} k_p^{1/2} + T_p \tag{6}$$

where,

$$T^+ = \frac{Pr_t}{k} \ln\left(Ey^+\right) + 9.24 Pr_t\left(\frac{Pr}{Pr_t} - 1\right)\left(\frac{Pr_t}{Pr}\right)^{1/4} \tag{7}$$

$$y^+ = \frac{\rho u_p C_\mu^{1/4} k_p^{1/2}}{\mu} \tag{8}$$

2.3 Numerical Procedures

A FLUENT code was used in this study, which was the thermofluid analysis code. Its computational algorithm was based on the SIMPLE method and the control volume approach was adopted to solve the governing equations (1)-(5) by a finite difference scheme. The convection and diffusion terms in the governing equations were discretized by using the power law and central differencing schemes, respectively. The discretized equations were solved by using a tri-diagonal matrix algorithm. The boundary coordinate fitted method[12] was adopted to generate arbitrary grid points which would fit the shape of analytical body surface. Using this method, the governing equations (1) - (5) are rewritten to the following equations (9) - (13), respectively.

◆ Continuity equation

$$\frac{\partial |J|\rho U_i}{\partial \xi_i} = 0 \tag{9}$$

◆ Raynolds averaged Navier-Stokes equation

$$\frac{1}{|J|}\frac{\partial |J|\rho U_j u_i}{\partial \xi_j} = -\frac{\partial \xi_j}{\partial x_i}\frac{\partial P_p}{\partial \xi_j} + \frac{1}{|J|}\frac{\partial}{\partial \xi_j}\left\{2|J|\frac{\partial \xi_j}{\partial x_k}\mu_{eff}S_{ik}\right\} + \beta - \frac{2}{3}\frac{\partial(\rho k)}{\partial \xi_j} \tag{10}$$

◆ Energy equation

$$\frac{1}{|J|}\frac{\partial |J|\rho U_j T}{\partial \xi_i} = \frac{1}{|J|}\frac{\partial}{\partial \xi_i}\left\{|J|g_{ij}\frac{\mu_{eff}}{Pr_{eff}}\frac{\partial T}{\partial \xi_j}\right\} \tag{11}$$

◆ k-equation

$$\frac{1}{|J|}\frac{\partial |J|\rho U_i k}{\partial \xi_i} = \frac{1}{|J|}\frac{\partial}{\partial \xi_i}\left\{|J|g_{ij}\frac{\mu_t}{\sigma_k}\frac{\partial k}{\partial \xi_j}\right\} + 2\mu_t S_{ij}\frac{\partial \xi_l}{\partial x_i}\frac{\partial u_j}{\partial \xi_l} - \rho\varepsilon \qquad (12)$$

◆ ε-equation

$$\frac{1}{|J|}\frac{\partial |J|\rho U_i \varepsilon}{\partial \xi_i} = \frac{1}{|J|}\frac{\partial}{\partial \xi_i}\left\{|J|g_{ij}\frac{\mu_t}{\sigma_\varepsilon}\frac{\partial k}{\partial \xi_j}\right\} + 2C_1\frac{\varepsilon}{k}\mu_t S_{ij}\frac{\partial \xi_l}{\partial x_i}\frac{\partial u_j}{\partial \xi_l} - C_2\rho\frac{\varepsilon^2}{k} \qquad (13)$$

Where,

$$U_i = \left(\partial \xi_i / \partial x_j\right)u_j \qquad (14)$$

$$J = \frac{\partial\left(x_1, x_2, x_3\right)}{\partial\left(\xi_1, \xi_2, \xi_3\right)} \qquad (15)$$

$$S_{ik} = \frac{1}{2}\left(\frac{\partial \xi_l}{\partial x_k}\frac{\partial u_i}{\partial \xi_l} + \frac{\partial \xi_l}{\partial x_i}\frac{\partial u_k}{\partial \xi_l}\right) \qquad (16)$$

$$g_{ij} = \nabla \xi_i \cdot \nabla \xi_j \qquad (17)$$

Here, x and ξ denote the physical domain (x_1, x_2, x_3) and calculation domain (ξ_1, ξ_2, ξ_3); where each subscript of i, j, k, l shows the Cartesian tensor notation and the values 1, 2, 3, respectively. Computational grid consisted of 46x9x52 points in x, y and z directions, and the decision for the grid number was based on Mastin and Thompson's assumptions[12].

To validate the calculation results of the turbulent heat transfer computed by the present numerical analysis, the author first calculated the same conditions as the experiment of Kays and Crawford[13] that was performed in the concentric smooth annulus with fully developed turbulent flow under the following conditions: a heated inner wall, an insulated outer wall, Di/Do=0.5, Pr=0.7 and Re=10^4, 3×10^4 and 10^5. In consequence, the calculated heat transfer coefficients were in excellent agreement with their experimental results with an error of less than 5%. Therefore, it was concluded that the k-ε turbulence model could be applied in the present numerical analysis.

3. RESULTS AND DISCUSSION

3.1 Flow Characteristics

Distributions of the predicted axial velocity, w, at $Re=5000$ are shown in Fig. 4 (a) for the inlet section of the computational domain and Fig. 4 (b) for the axial mid-position between the inlet and outlet sections. In Fig. 4 (a), w decreased in the center region and increased as θ approached both circumferential ends. This predicted result implies that the fluid flow could not fully develop in the center region where the periodic spacer ribs were set axially in a row. In Fig. 4 (b), w at the spacer rib position became zero, and w except for that position was accelerated because of a channel reduction resulting from the spacer rib.

Figure 5 represents the predicted axial velocity distribution at the center plane between the inner and outer walls of the spacer-ribbed fuel channel at $Re=5000$. Here, the white area at the middle in this figure means the spacer rib position and every velocity was zero on the rib surface. The velocity decreased along the spacer rib line because the velocity defect occurred after the spacer rib. Although the decreased velocity recovered as the axial distance increased, the fluid received an influence from the next spacer rib that was arranged axially in a row on the external surface of the fuel rod before the flow could fully developed. In addition, the velocity increased circumferentially around the spacer rib because of the channel blockage effect.

Distributions of the predicted turbulence kinematic energy, k, in the axial direction at $Re=5000$ can be seen in Fig. 6. In the figure, (a) shows the k distribution of near the inner wall location, (b) the center plane between the inner and outer walls, and (c) near the outer wall location. In Fig. 6 (a), k indicated a lower value along the free shear flow generated after the spacer rib as can be seen as a couple of lines. On the other hand, it indicated a higher value at the side position of the spacer rib in the circumferential direction. In Fig. 6 (b), k in the turbulence core region had its maximum value at the side position of the spacer rib where a highly turbulent shear layer was generated. In this case, k except for around the spacer rib was almost equal to $0.62 \text{ m}^2/\text{s}^2$, and then, it showed that the large turbulence did not exist in the region except for around the spacer rib. In Fig. 6 (c), k decreased at the locations before and after the spacer rib such as an axial groove, and k at these locations were more than 20% lower than k at an environment of about $2 \text{ m}^2/\text{s}^2$. The same tendencies as the numerical results from Figs. 6 (a) to (c) were also observed for the other Reynolds numbers.

Figure 7 shows the variation in the friction factor, f, with Re in the spacer-ribbed fuel channel in the fully developed flow region. Here, the open squares and circles indicate the

experimental results under the heated and isothermal flow conditions, respectively, and the solid circles represent the numerical predictions.   The f in the experiments was calculated from

$$f = De\left[\Delta P - (\rho_o w_o^2 - \rho_i w_i^2)\right]/\ 2L\rho\overline{w}^2 \tag{18}$$

Here, ΔP is the measured pressure loss; $(\rho_o w_o^2 - \rho_i w_i^2)$ the acceleration loss caused by the volumetric expansion of the heated gas; L the subrod length of the simulated fuel rod and $\overline{w}$ the mean axial velocity; respectively; and the term of $(\rho_o w_o^2 - \rho_i w_i^2)$ is negligible under the isothermal flow condition.   Broken line in the figure indicates the Blasius equation for a concentric smooth annulus.

As shown in Fig. 7, a difference between the heated and isothermal experimental results was small and those results were in good agreement with the following empirical correlation expressed as the solid line over the range of $Re{>}2000$.

$$f = 0.1 Re^{-0.25}(Tk_w/Tk_b)^{-0.5}\ ;\ \ Re{>}2000 \tag{19}$$

The maximum deviation between the experimental data and Eq. (19) was 15%.   The f in the spacer-ribbed fuel channel was higher than that of the concentric smooth annulus in the turbulent region.   It is evident that the friction factor increased as a result of the channel blockage effect and the turbulence promoter effect due to the spacer ribs.

On the other hand, the wall shear stress, τ_w, was expressed from the concept of the log-law wall function under the turbulent flow condition, and is shown as:

$$\tau_w = \frac{\rho u_p C_\mu^{1/4} k_p^{1/2} \kappa}{\ln(Ey^+)} \tag{20}$$

Therefore, f was predicted numerically by

$$f = \tau_w\ /\ (\rho\ \overline{w}^2\ /\ 2) \tag{21}$$

Consequently, it was confirmed that the friction factor predicted by Eq. (21) agreed with that obtained from Eq. (19) within an error of less than 11%; and then, it was considered that the present numerical analyses had the sufficient accuracy for predicting the friction factors in the spacer-ribbed fuel channel.

3.2 Heat Transfer Characteristics

Predicted inner wall temperature, T_{iw}, at Re=5000 is shown in Fig. 8. The T_{iw} indicates the lowest value at both circumferential ends of θ =60° and -60°. The reason is as follows: The reduction in the channel cross-section due to the spacer rib increases the velocity, and the velocity becomes maximum at the center position between the spacer ribs set in the circumferential direction. As a consequence, the heat transfer coefficient in the spacer-ribbed channel is improved in comparison with that in the smooth annulus. On the other hand, T_{iw} increases circumferentially from both ends of θ =60° and -60° to θ =0°. Then, T_{iw} at θ =0° is influenced by the wake flow generated by the spacer rib and greatly reduced at a certain position just after the spacer rib. Therefore, it was considered that the heat transfer coefficients were augmented at that position. On the other hand, it is expected that the spacer rib operates as a cooling fin. However, the surface area of one spacer rib was less than 1% in comparison with that of one fuel rod, and then it was concluded that the cooling fin effect by the spacer rib was scarcely expected in the present case.

Figure 9 shows the variation of q_r / q_e with Re for different axial locations of z/De. Here, q_r / q_e represents the ratio of radiative heat flux to total heat flux and z/De is the dimensionless axial distance from the inlet of the spacer-ribbed fuel channel. In addition, the open symbol denotes the experimental data and the solid symbol the numerical predictions at z/De=290. The q_r from the inner to the outer walls is calculated by

$$q_r = \sigma\left(Tk_{iw}^4 - Tk_{ow}^4\right)\left[\frac{1}{e_{iw}} + \frac{Di}{Do}\left(\frac{1}{e_{ow}} - 1\right)\right]^{-1} \tag{22}$$

Here, $Tk_{iw}=T_{iw}+273.15$, $Tk_{ow}=T_{ow}+273.15$, e_{iw} and e_{ow} denote the emissivities for the fuel rod surface and for the outer tube wall. For the temperature range in this study, e_{iw} and e_{ow} are 0.8[9] for graphite and 0.3[10] for Incolloy 800H. The q_r / q_e increased as z/De was increased because the temperature level became high, and it reached more than 10% when Re<2500 at z/De=290. It was found that the numerical predictions were in good agreement with the experimental data at z/De=290.

The predicted local heat transfer coefficient, α, on the inner wall at Re=5000 can be seen in Fig. 10. The α is calculated by $\alpha = q_c$ / $(T_{iw} - \overline{T}_b)$; $\overline{T}_b$ is the average bulk temperature in the computational domain; and q_c is the convective heat flux and shown as $q_c = q_e - q_r$. Here, the white area at the middle position in this figure shows the spacer rib position. In general, α is in inverse proportion to the T_{iw} value if q_c and $\overline{T}_b$ are constant. Therefore, as can be anticipated from the T_{iw} distribution in Fig. 8, it was shown that α was the largest at θ =60° and -60° along the flow direction, and the higher heat transfer region can be seen at a certain

position just after the spacer rib due to the effect of heat transfer augmentation as a result of the turbulence promoter.

Figure 11 shows the relation between Nusselt number, Nu, and Re in the fully developed flow region. Here, the open symbol denotes Nusselt number on the inner wall in the spacer-ribbed fuel channel obtained from the experimental data. The broken line represents the empirical correlations of the heat transfer coefficients for the concentric smooth annulus, Nu_s, proposed by Dalle Donne and Meerwald[2] in the range of $Re \geq 7000$, Fujii, et al.[14] in $2700 < Re < 7000$ and Kays and Crawford[13] in $Re \leq 2700$. Those are expressed by the following equations:

$$Nu_s = 0.018(Di/Do)^{-0.16}Re^{0.8}Pr^{0.4} \quad ; \quad Re \geq 7000 \qquad (23)$$

$$Nu_s = 0.084(Re^{2/3} - 110)Pr^{0.4} \quad ; \quad 2700 < Re < 7000 \qquad (24)$$

$$Nu_s = 5.6 \quad ; \quad Re \leq 2700 \qquad (25)$$

The Nu was about 25% higher than Nu_s in the laminar region, 20% higher in the turbulent region and a maximum 100% higher in the transition region. Regarding the reason for the heat transfer augmentation, it is mainly considered that the spacer ribs effectively contributed as turbulence promoters. In addition, as Re decreased from the turbulent to the laminar region, the following special feature was observed: Nu_s decreased suddenly as soon as Re became less than about 7000; however, Nu decreased linearly with Re. This means that the transition region of the spacer-ribbed fuel channel was very short in comparison with the concentric smooth annulus. Consequently, the following empirical correlations on the heat transfer coefficients in the spacer-ribbed fuel channel were derived from the experimental data in the turbulent and laminar regions.

$$Nu = 0.0222Re^{0.8}Pr^{0.4} \quad ; \quad Re > 2000 \qquad (26)$$

$$Nu = 7.0 \quad ; \quad Re \leq 1800 \qquad (27)$$

Eqs. (26) and (27) shown by the solid lines in Fig. 11 agreed well with the experimental data with the deviation of less than $\pm 15\%$. Here, as seen in Eq. (26), the experimental data in the turbulent and transition region were arranged using $Pr^{0.4}$ corresponding to the cases of Eqs. (23) and (24).

The predicted average Nusselt number, $\overline{Nu}$, represented as the solid circle in Fig. 11, was calculated by dividing the total heat transfer from the heated walls, Q_w, by a sum over the heated wall cells in the heat transfer area multiplied by the temperature difference for each cell. It is written as:

$$\overline{Nu} = Q_w \Big/ \sum_{n=1}^{nl} \Big[B_n \big(T_{w,n} - \overline{T}_b \big) \Big] \tag{28}$$

Here, n is the cell number, nl the total cell number of the heated wall and B_n the heat transfer area in the heated wall. The $\overline{Nu}$ agreed well with Eq. (26) with an error of less than 15% in the region of $3000 \leq Re \leq 20000$. Therefore, it was concluded that the augmented heat transfer coefficients in the spacer-ribbed fuel channel were predicted numerically by the present numerical analyses and its accuracy was sufficient from a viewpoint of engineering.

4. CONCLUSIONS

The heat transfer characteristics in the spacer-ribbed fuel channel were analyzed numerically by 3-dimensional computations using the improved k-ε turbulence model constants and the boundary coordinate fitted method in a fully developed turbulent flow under the HTTR coolant conditions. The numerical predictions for the heat transfer coefficients and friction factors were compared with the experimental results. These results are summarized as follows.

1) The predicted turbulent heat transfer coefficients and predicted friction factors in the spacer-ribbed fuel channel were in good agreement with the experimental results, and consequently it was validated that the thermal-hydraulic performance of the spacer-ribbed fuel rod in the range of $3000 \leq Re \leq 20000$ could simulate sufficiently using the present numerical procedures and the improved k-ε turbulence model constants.

2) The mechanism for the heat transfer augmentation in the spacer-ribbed fuel channel was clarified quantitatively by the present numerical predictions. The main reason that turbulent heat transfer coefficients and friction factors in the spacer-ribbed fuel channel increased to around 20% in comparison with those in the concentric smooth annuls was due to both effects of the heat transfer augmentation caused by the spacer rib as the turbulence promoter and the axial velocity increase caused by the reduction in the channel cross-section.

3) The axial velocity decreased axially along the spacer-rib line because the velocity defect took place after the spacer rib. The decreased velocity recovered gradually as the axial distance increased, however, the fluid flow reached the next spacer rib located on the fuel rod surface before it became a fully developed flow. Therefore, it was found that the effect of the velocity defect continued over the flow direction in the spacer-ribbed fuel channel under the present spacer rib arrangement.

$$\overline{Nu} = Q_w / \sum_{n=1}^{nl} \left[B_n \left(T_{w,n} - \overline{T_b} \right) \right] \tag{28}$$

Here, n is the cell number, nl the total cell number of the heated wall and B_n the heat transfer area in the heated wall. The $\overline{Nu}$ agreed well with Eq. (26) with an error of less than 15% in the region of $3000 \leq Re \leq 20000$. Therefore, it was concluded that the augmented heat transfer coefficients in the spacer-ribbed fuel channel were predicted numerically by the present numerical analyses and its accuracy was sufficient from a viewpoint of engineering.

4. CONCLUSIONS

The heat transfer characteristics in the spacer-ribbed fuel channel were analyzed numerically by 3-dimensional computations using the improved k-ε turbulence model constants and the boundary coordinate fitted method in a fully developed turbulent flow under the HTTR coolant conditions. The numerical predictions for the heat transfer coefficients and friction factors were compared with the experimental results. These results are summarized as follows.

1) The predicted turbulent heat transfer coefficients and predicted friction factors in the spacer-ribbed fuel channel were in good agreement with the experimental results, and consequently it was validated that the thermal-hydraulic performance of the spacer-ribbed fuel rod in the range of $3000 \leq Re \leq 20000$ could simulate sufficiently using the present numerical procedures and the improved k-ε turbulence model constants.

2) The mechanism for the heat transfer augmentation in the spacer-ribbed fuel channel was clarified quantitatively by the present numerical predictions. The main reason that turbulent heat transfer coefficients and friction factors in the spacer-ribbed fuel channel increased to around 20% in comparison with those in the concentric smooth annuls was due to both effects of the heat transfer augmentation caused by the spacer rib as the turbulence promoter and the axial velocity increase caused by the reduction in the channel cross-section.

3) The axial velocity decreased axially along the spacer-rib line because the velocity defect took place after the spacer rib. The decreased velocity recovered gradually as the axial distance increased, however, the fluid flow reached the next spacer rib located on the fuel rod surface before it became a fully developed flow. Therefore, it was found that the effect of the velocity defect continued over the flow direction in the spacer-ribbed fuel channel under the present spacer rib arrangement.

ACKNOWLEDGMENT

NOMENCLATURE

B = heat transfer area (m^2)

c_p = specific heat of the fluid (J/kgK)

Di = inner diameter (m)

De = hydraulic diameters (m)

Do = outer diameter (m)

E = log-law constant

e = emissivity

f = friction factor

G = flow rate (kg/s)

H = channel height (H=De/2) (m)

k = turbulence kinematic energy (m^2/s^2)

L = subrod length (m)

Nu = Nusselt number

$\overline{Nu}$ = average Nusselt number

P, ΔP = pressure, differential pressure (Pa)

Pr = Prandtl number

Pr_t = turbulent Prandtl number

q^+ = dimensionless heat flux

Q = heat transfer rate

Q_e = electric power of fuel rod (kW)

q_c = convective heat flux (W/m^2)

q_e = total heat flux (W/m^2)

q_r = radiative heat flux (W/m^2)

q_w = wall heat flux (W/m^2)

Re = Reynolds number (Re=$\overline{w}$De/v)

T, $\overline{T}$ = temperature (°C) and average temperature (°C)

Tk = absolute temperature (K)

u, v, w = circumferential, radial, and axial velocities (m/s)

x, y, z = circumferential, radial, and axial coordinates

ACKNOWLEDGMENT

NOMENCLATURE

B = heat transfer area (m^2)

c_p = specific heat of the fluid (J/kgK)

Di = inner diameter (m)

De = hydraulic diameters (m)

Do = outer diameter (m)

E = log-law constant

e = emissivity

f = friction factor

G = flow rate (kg/s)

H = channel height (H=De/2) (m)

k = turbulence kinematic energy (m^2/s^2)

L = subrod length (m)

Nu = Nusselt number

$\overline{Nu}$ = average Nusselt number

P, ΔP = pressure, differential pressure (Pa)

Pr = Prandtl number

Pr_t = turbulent Prandtl number

q^+ = dimensionless heat flux

Q = heat transfer rate

Q_e = electric power of fuel rod (kW)

q_c = convective heat flux (W/m^2)

q_e = total heat flux (W/m^2)

q_r = radiative heat flux (W/m^2)

q_w = wall heat flux (W/m^2)

Re = Reynolds number (Re=$\overline{w}$De/ν)

T, $\overline{T}$ = temperature (°C) and average temperature (°C)

Tk = absolute temperature (K)

u, v, w = circumferential, radial, and axial velocities (m/s)

x, y, z = circumferential, radial, and axial coordinates

y = distance from the wall (m)

y^+ = dimensionless distance from the wall

Greek

α = heat transfer coefficient (W/m²K)

β = pressure drop parameter (Pa/m)

ε = dissipation rate of turbulence (m²/s³)

κ = von Karman's constant

λ = thermal conductivity (W/mK)

μ, μ_t = viscosity, turbulent viscosity (Pa s)

v = kinematic viscosity (m²/s)

θ = sector angle (°)

ρ = density (kg/m³)

τ_w = wall shear stress (Pa)

Subscripts

b = bulk

i, o = in and out

iw, ow, w= inner wall, outer wall and wall

s = smooth

REFERENCES

1. W. M. KAYS and E. Y. LEUNG, "Heat Transfer in Annular Passages - Hydrodynamically Developed Turbulent Flow with Arbitrarily Prescribed Heat Flux", *Int. J. Heat Mass Transfer*, **6**, 537(1962).

2. M. DALLE DONNE and E. MEERWALD, "Heat Transfer and Friction Coefficients for Turbulent Flow of Air in Smooth Annuli at High Temperature", *Int. J. Heat Mass Transfer*, **16**, 787(1973).

3. N. W. WILSON, and J. O. MEDWELL, "An Analysis of Heat Transfer for Fully Developed Turbulent Flow in Concentric Annuli", *ASME J. Heat Transfer*, **90**, 43(1968).

4. M. DALLE DONNE and L. MEYER, "Turbulent Convective Heat Transfer from Rough Surfaces with Two-Dimensional Rectangular Ribs", *Int. J. Heat Mass Transfer*, **20**, 583(1977).

5. M. A. HASSAN and K. REHME, Hassan, "Heat Transfer Near Spacer Grids in Gas-Cooled Rod Bundles", *Nuclear technology*, **52**, 401(1981).

6. K. TAKASE, "Experimantal Results of Heat Transfer Coefficients and Friction Factors in a 2D/3D Rib-Roughened Annulus", *Experimental Thermal and Fluid Sciences*, to be published.

7. W. P. JONES and B. E. LAUNDER, "The Prediction of Laminarization with a Two-Equation Model of Turbulence", *Int. J. Heat Mass Transfer*, **15**, 301(1972).

8. S. V. PATANKAR, C. H. LIU, and E. M. SPARROW, "Fully Developed Flow and Heat Transfer in Ducts Having Streamwise-Periodic Variations of Cross-Sectional Area", *ASME J. Heat Transfer*, **99**, 180(1977).

9. A. GOLDSMITH, T. E. WATERMAN, and H. J. HIRSCHBORN, "Handbook of Thermophysical Properties of Solid Materials", MaCMILAN, NY, **1**, 127(1961).

10. T. MAKINO, T. KUNITOMO, and T. MORI, "Study on Characteristics of Thermal Radiation of Heat Resisting Alloy with High Temperature", *Trans. of JSME Series B*, **49**, 441, 1040(1983).

11. B. E. LAUNDER and D. B. SPALDING, "The Numerical Computation of Turbulent Flows", *Computer Methods in Applied Mechanics and Engineering*, **3**, 269(1974).

12. C. W. MASTIN and J. F. THOMPSON, "Transformation of Three-Dimensional Regions onto Rectangular Regions by Elliptic Systems", *Numerische Mathematik*, **29**, 397(1978).

13. W. M. KAYS and M. E. CRAWFORD, "Convective Heat and Mass Transfer", 3rd edition, McGraw-Hill, NY, 123(1993).

14. S. FUJII, M. HISHIDA, H. KAWAMURA, and N. AKINO, "Heat Transfer in Annular Channels under the High Heat Flux Conditions", *17th Japan Heat Transfer Symposium*, **A213**, 97(1980).
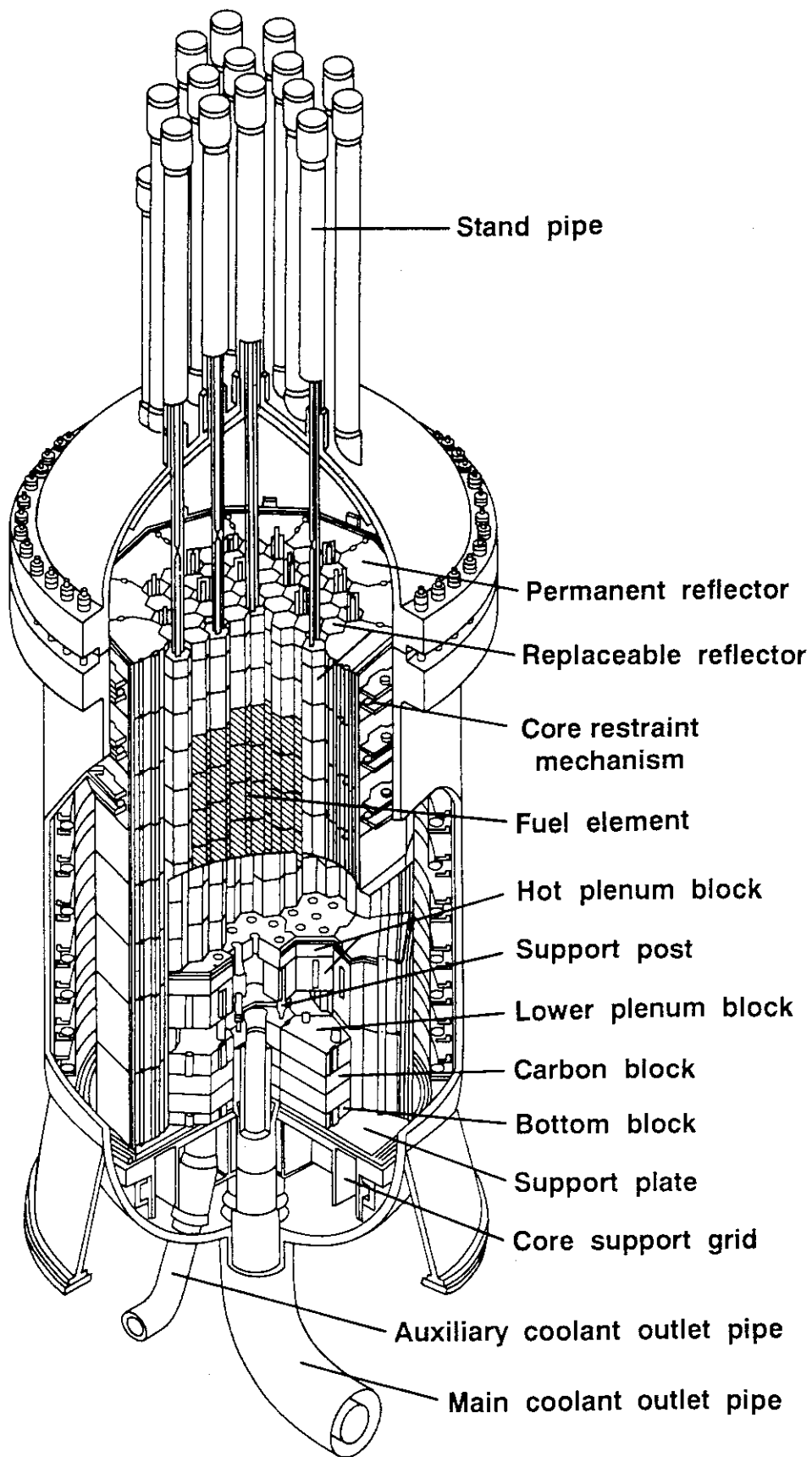
Fig. 1 Structural drawing in the HTTR pressure vessel: Helium gas flows
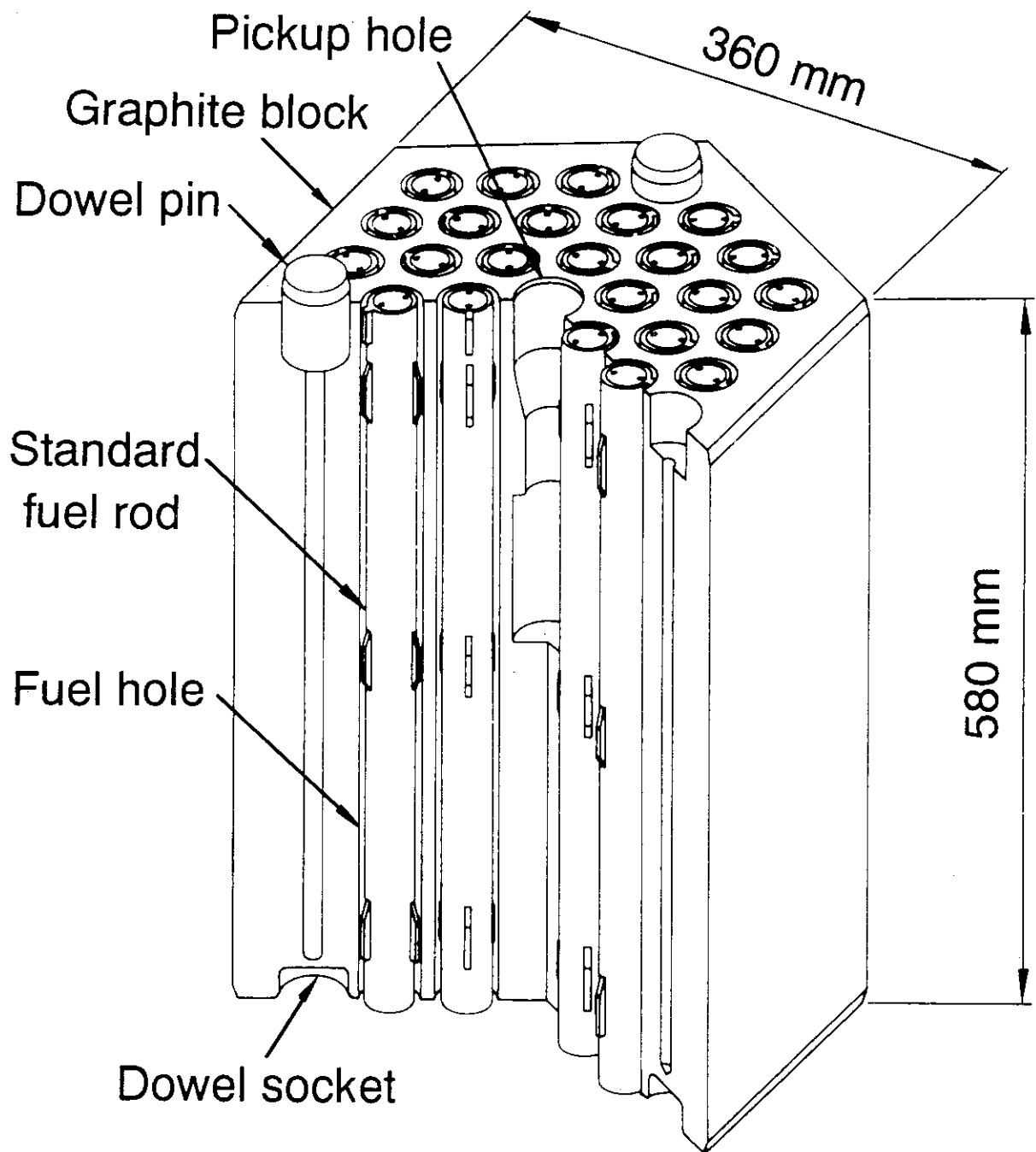downward through the reactor core in the pressure vessel.
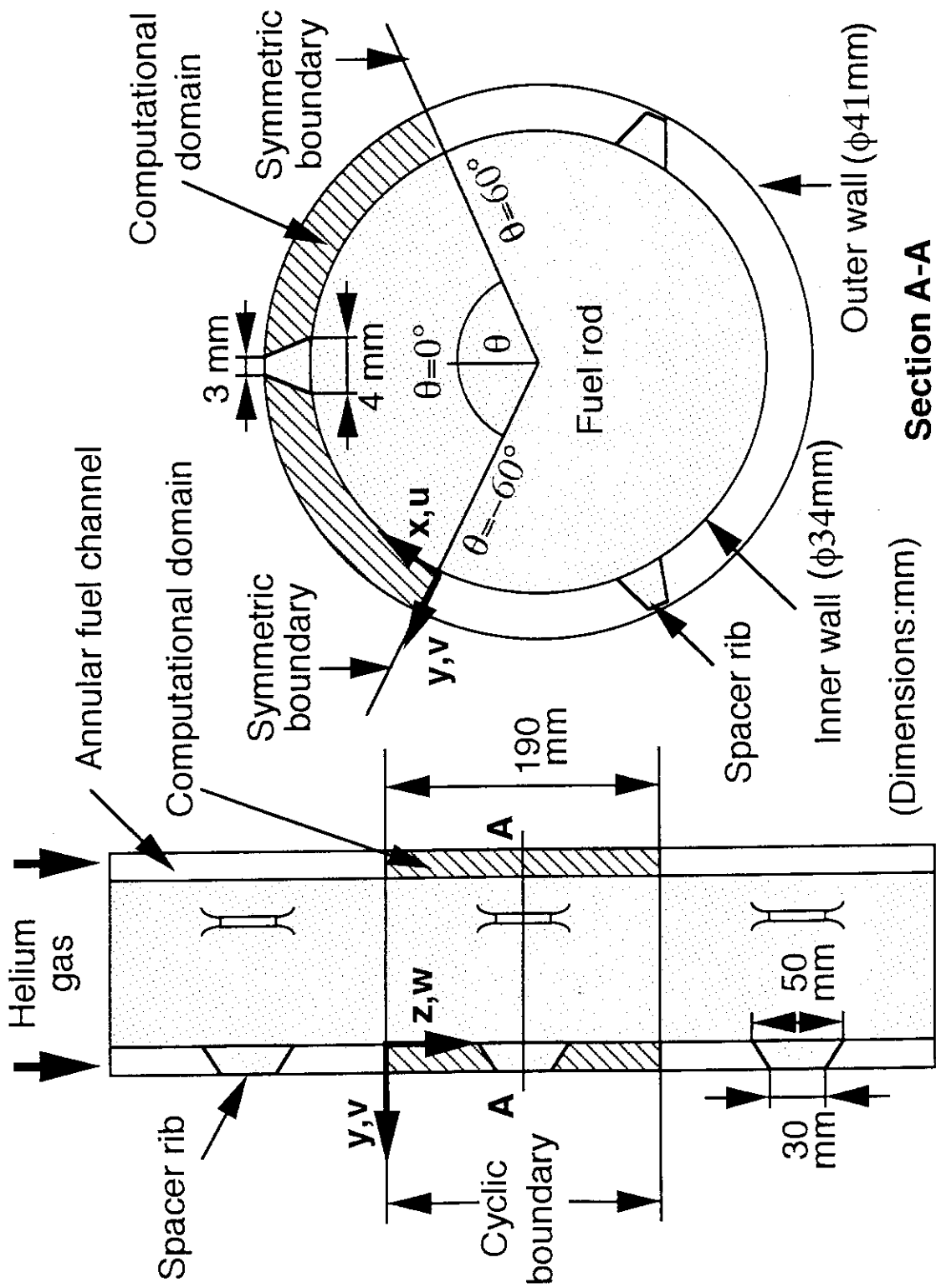
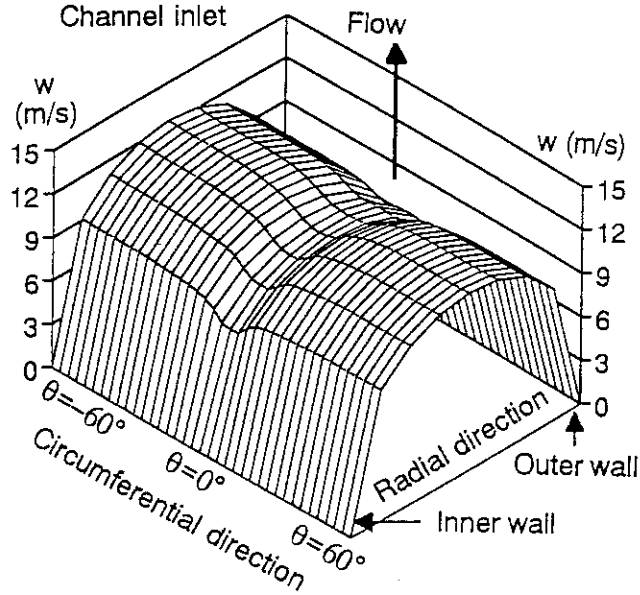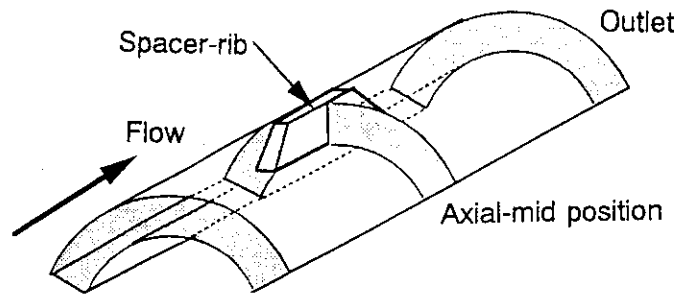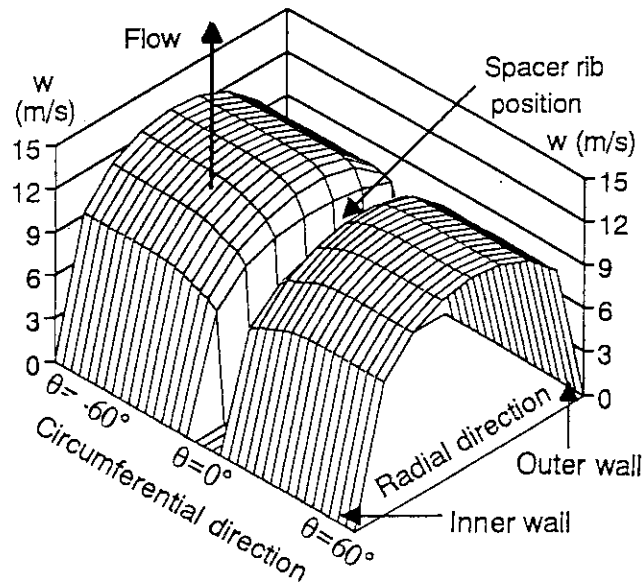Fig. 2 The HTTR fuel element with 33 standard fuel rods.

Fig. 3　Computational model and boundary conditions.

(a) Inlet section

(b) Axial mid-position

Fig. 4 Predicted axial velocity distributions between the inner and outer walls at Re=5000:
(a) Inlet section of the computational domain and
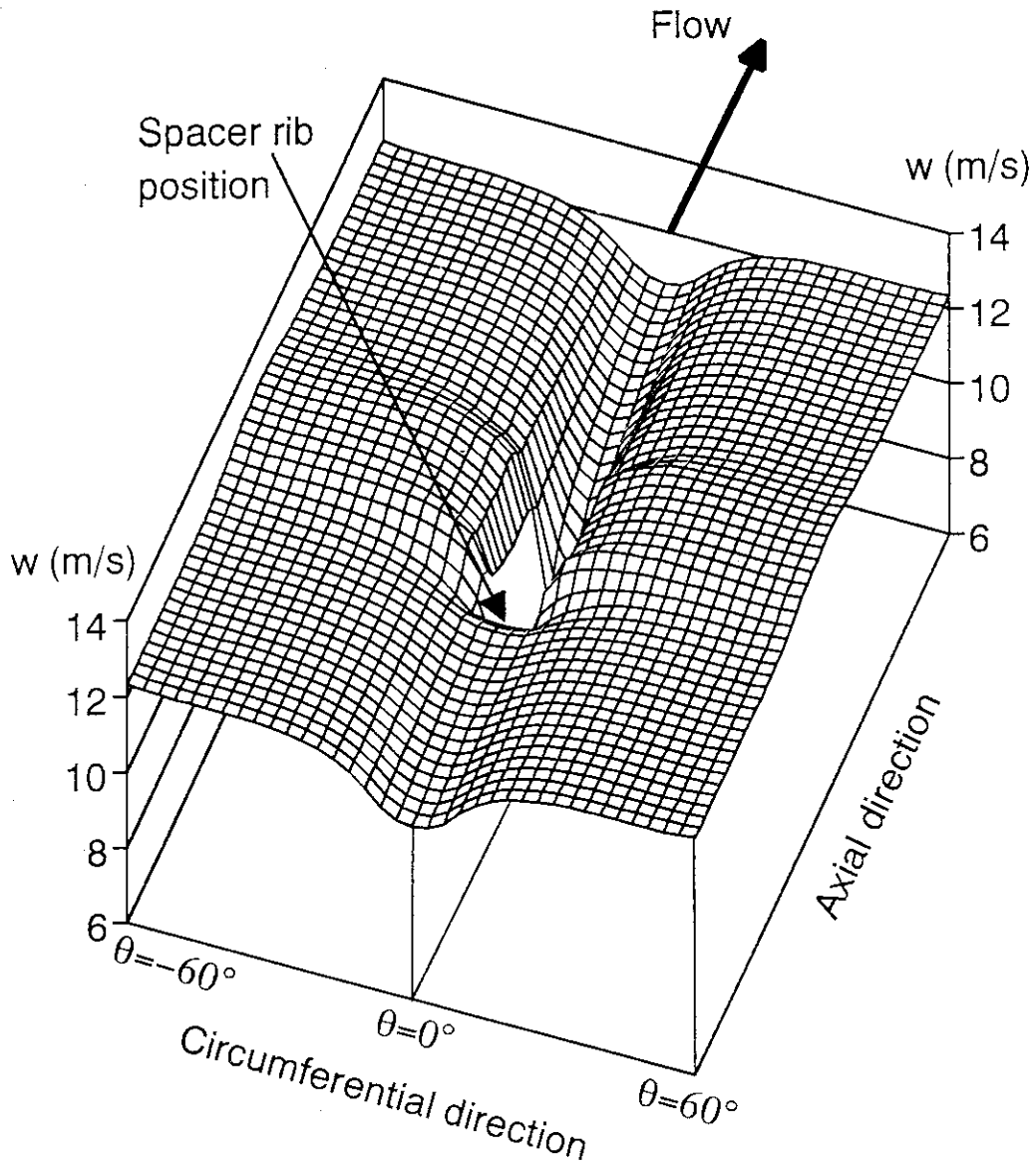(b) Axial mid-position between the inlet and outlet sections.

Fig. 5 Predicted axial velocity distribution in the center plane between the inner and outer walls at Re=5000.

(a) Near the inner wall

(b) Center plane between the walls

(c) Near the outer wall
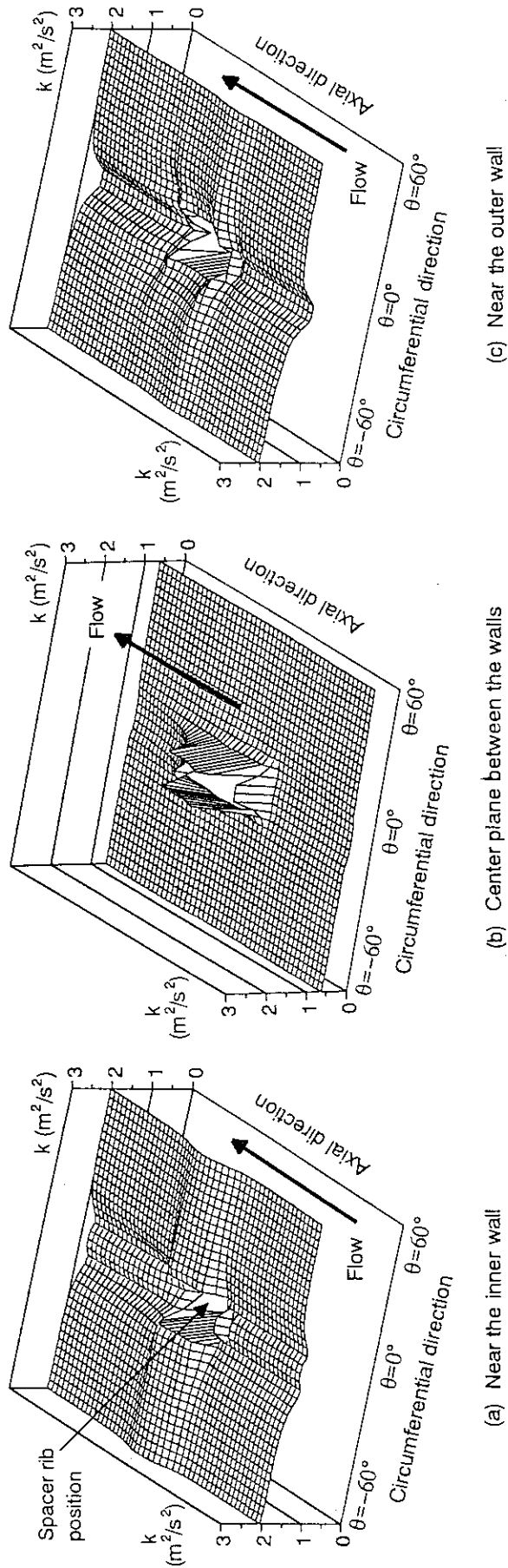
Fig. 6 Predicted turbulence kinematic energy distributions along the axial direction at Re=5000: (a) Near the inner wall, (b) Center plane between the walls, and (c) Near the outer wall.
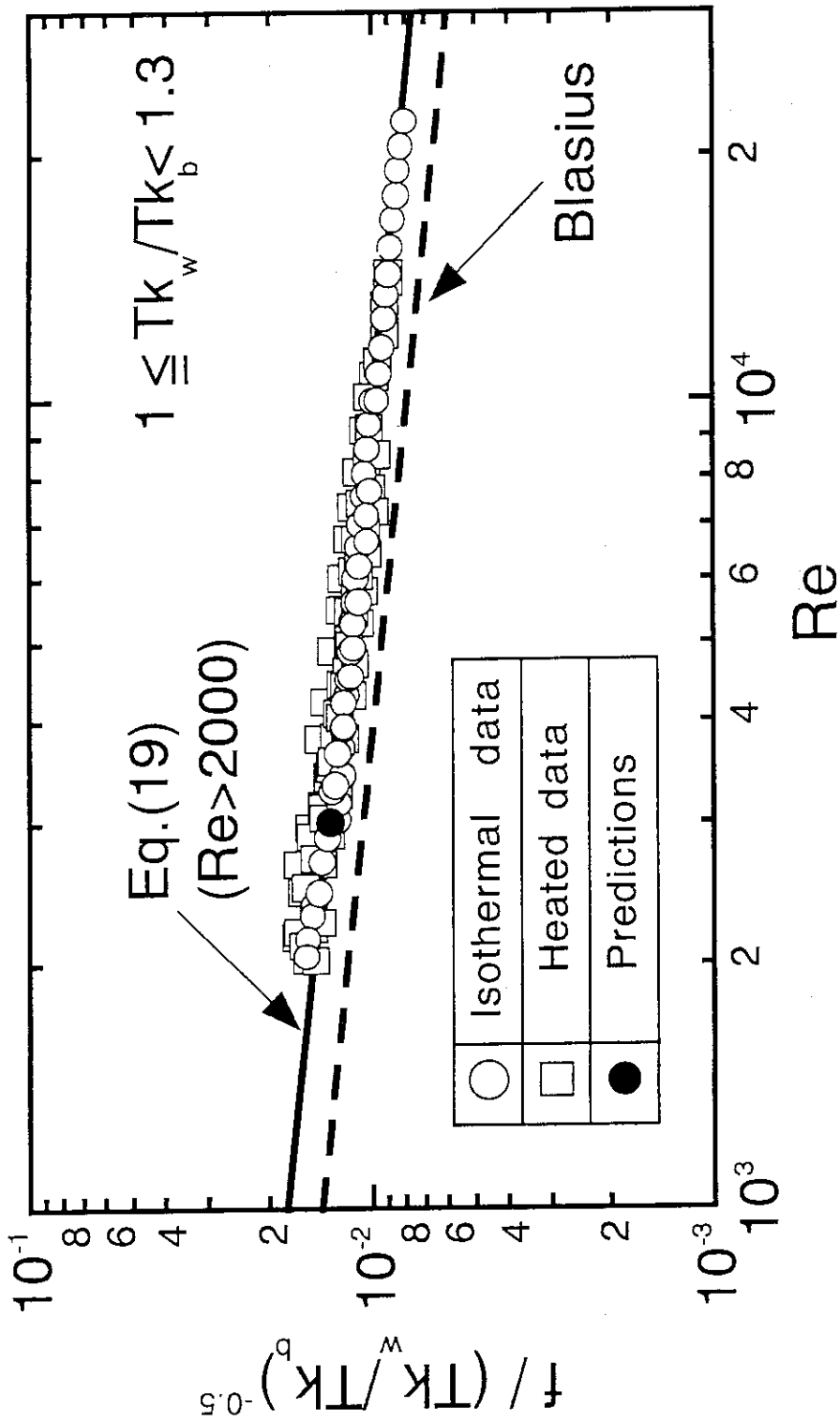
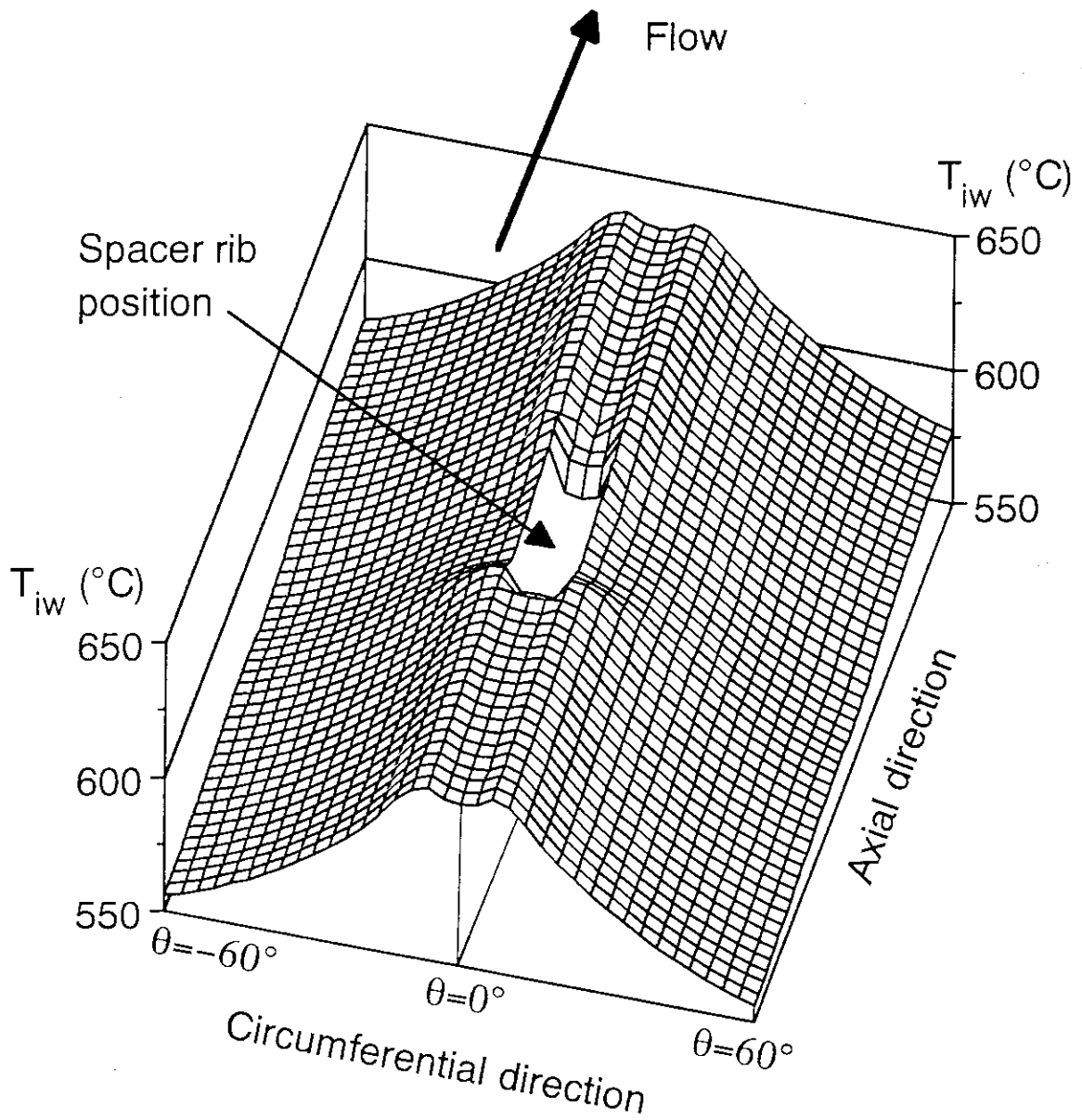Fig. 7 Comparison of the predicted friction factors with the experimental results.

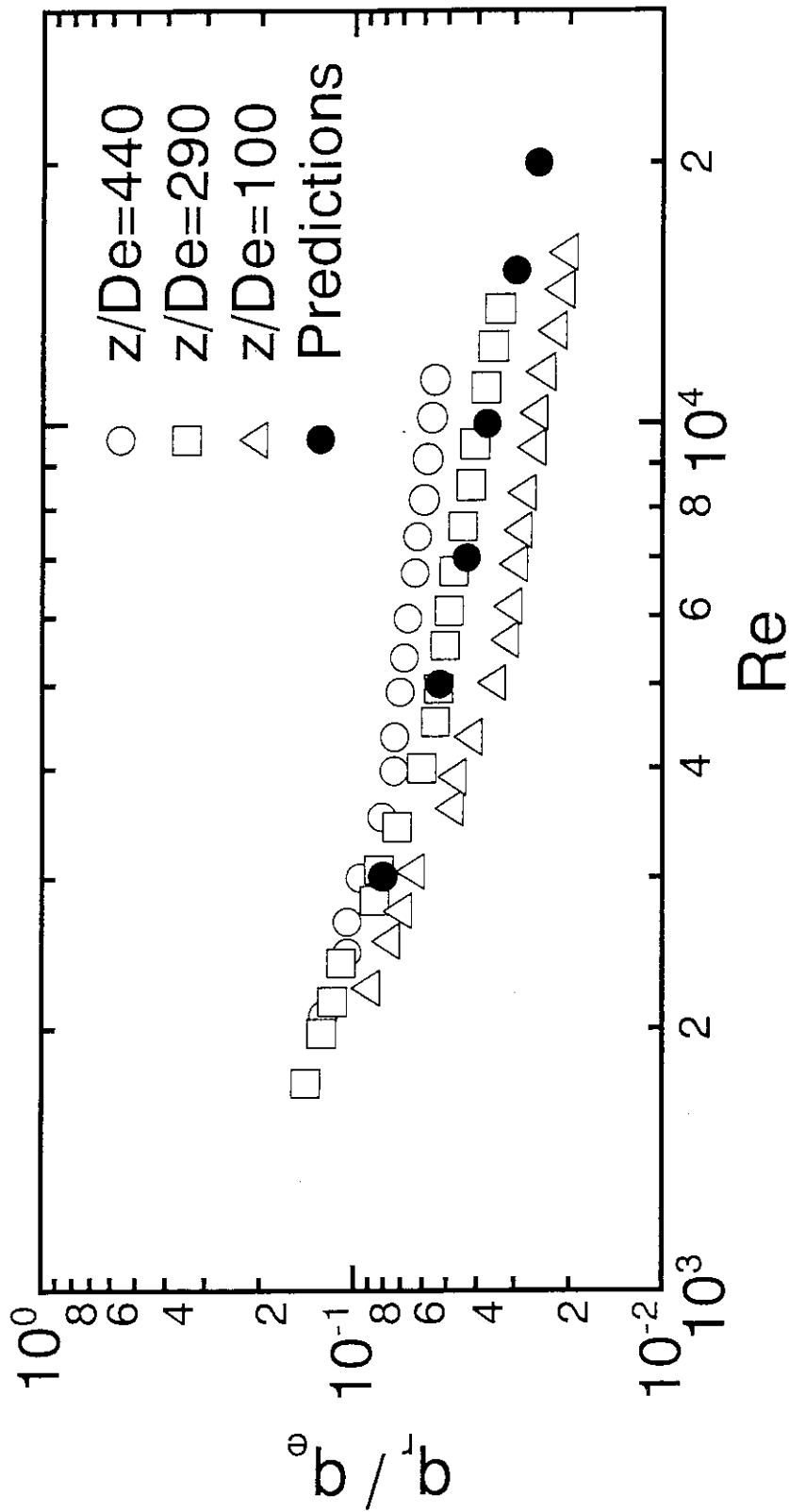Fig. 8 Predicted inner wall temperature distribution at Re=5000.

Fig. 9 Comparison of the predicted radiative heat flux rates with the experimental results for different axial locations of z/De.
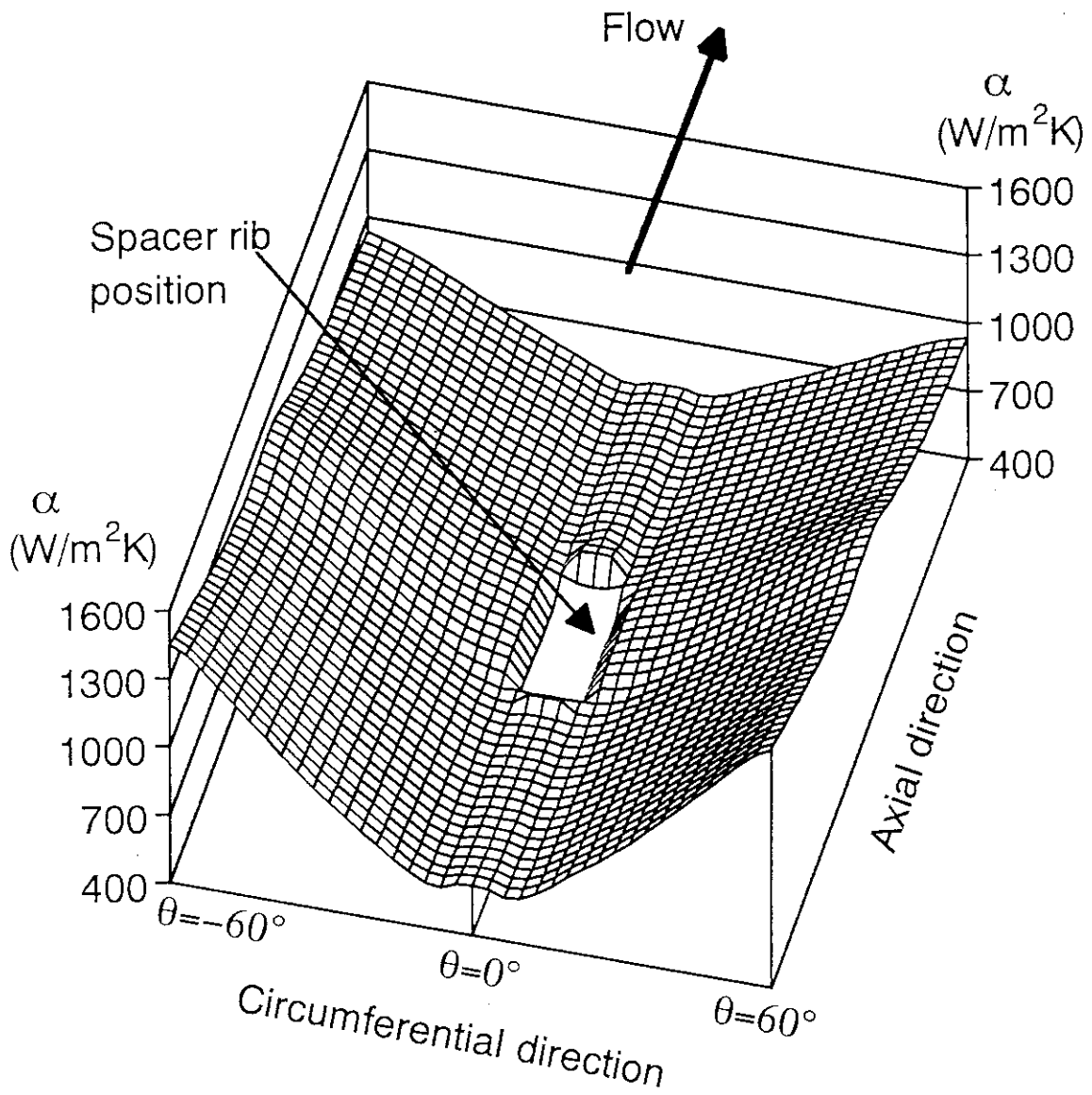
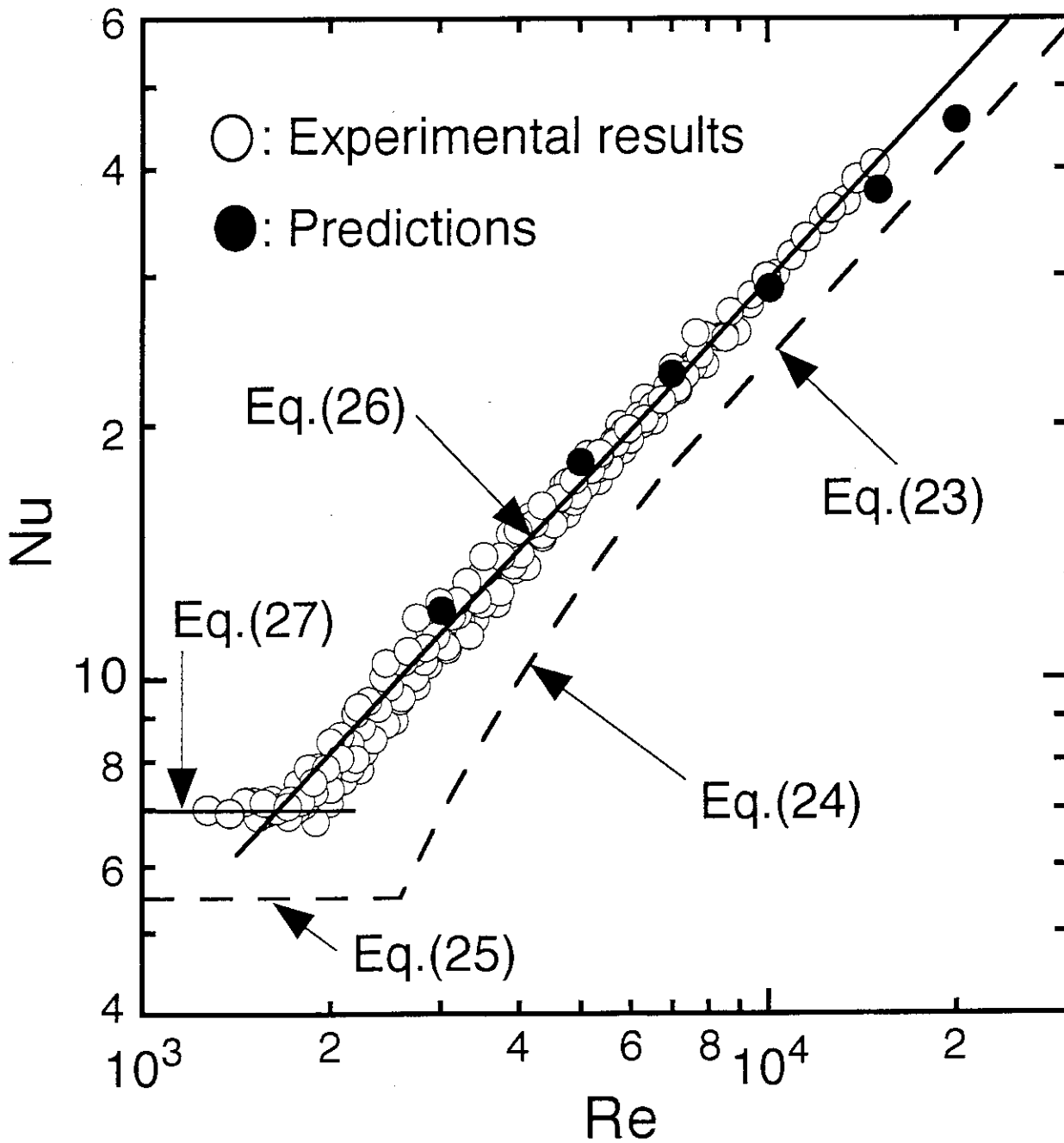Fig. 10 Predicted local heat transfer coefficients on the inner wall at Re=5000.

Fig. 11 Comparison of the predicted average Nusselt numbers with the experimental results.